Journal of Magnetic Resonance **146,** 345–358 (2000)
doi:10.1006/jmre.2000.2125, available online at http://www.idealibrary.com on IDEAL®

Slow-Motion Theory of Nuclear Spin Relaxation in Paramagnetic Low-Symmetry Complexes: A Generalization to High Electron Spin

T. Nilsson and J. Kowalewski[1]

Division of Physical Chemistry, Arrhenius Laboratory, Stockholm University, S-106 91 Stockholm, Sweden

E-mail: jk@physc.su.se

Received February 24, 2000; revised May 17, 2000

The slow-motion theory of nuclear spin relaxation in paramagnetic low-symmetry complexes is generalized to comprise arbitrary values of *S*. We describe the effects of rhombic symmetry in the static zero-field splitting (ZFS) and allow the principal axis system of the static ZFS tensor to deviate from the molecule-fixed frame of the nuclear-electron dipole–dipole tensor. We show nuclear magnetic relaxation dispersion (NMRD) profiles for different illustrative cases, ranging from within the Redfield limit into the slow-motion regime with respect to the electron spin dynamics. We focus on $S = 3/2$ and compare the effects of symmetry-breaking properties on the paramagnetic relaxation enhancement (PRE) in this case with that of $S = 1$, which we have treated in a previous paper. We also discuss cases of $S = 2$, 5/2, 3, and 7/2. One of the main objectives of this investigation, together with the previous papers, is to provide a set of standard calculations using the general slow-motion theory, against which simplified models may be tested.

Key Words: **high-spin systems; paramagnetic; relaxation; slow-motion; zero-field splitting.**

INTRODUCTION

The presence of unpaired electrons in transition-metal complexes has profound effects on the nuclear spin relaxation of ligand nuclei, which experience a paramagnetic relaxation enhancement (PRE). The field dependence of the PRE, which is usually presented as a nuclear magnetic relaxation dispersion (NMRD) profile, reveals information about microscopic structural and dynamic properties of the investigated nucleus but also indirectly about the electron spin system (*1–5*). In this paper we are interested in the PRE of ligand protons (e.g., in water molecules) in paramagnetic low-symmetry transition-metal complexes of $S = 1, 3/2, 2, 5/2, 3$, and 7/2, exchanging rapidly with the bulk. Systems of low symmetry have a static zero-field splitting (ZFS) interaction present, which at low magnetic field (i.e., when the electron spin Zeeman interaction is weak compared to the ZFS) dominates the characteristics of the NMRD profiles.

The conventional theory by Solomon, Bloembergen, and Morgan (SBM) (*6–9*), or rather the modified Solomon–Bloembergen (MSB) equations (*1–3*), do not include the static ZFS interaction. The SBM theory is thus inapplicable to interpreting NMRD profiles for low-symmetry complexes unless the magnitude of the electron spin Zeeman interaction is much larger than that of the static ZFS interaction (i.e., the high-field limit). Strandberg and Westlund (*10*) have recently modified the MSB equations to include the static ZFS, and also the hyperfine coupling to the metal nucleus, but still under the assumption that the electron spin Zeeman interaction is much larger than the static ZFS.

The general slow-motion theory of nuclear spin relaxation in paramagnetic systems developed by Kowalewski and co-workers (*11–15*) can handle complexes of any symmetry, for any electron spin *S*, at various magnetic fields, and with arbitrary magnitudes of the different interactions present (e.g., static and transient ZFS). The slow-motion theory is based on the stochastic Liouville equation, using Liouville space superoperator formalism (*16, 17*), where the nuclear spin system is treated on a Redfield theory level (*18–22*), but where the electron spin system is treated together with classical degrees of freedom as a composite lattice (see the theory section). We will assume that the primary mechanism for the electron spin relaxation is by distortional modulation of a transient ZFS interaction due to collisions with solvent molecules. This mechanism is described by the so-called pseudorotation model, which may be pictured as an ellipsoid diffusing on the unit sphere. The mechanisms related to the static ZFS and the Zeeman interactions modulated by reorientation are also included. Since the magnitude of the transient ZFS can, in the present formalism, take any value, this means that the slow-motion theory allows the electron spin relaxation to be outside of the Redfield limit. The extension to the slow-motion regime for the electron spin relaxation is possible because no electron spin relaxation times are explicitly defined.

In a previous paper (*23*), which in the following will be referred to as paper I, we investigated symmetry-breaking properties for $S = 1$ complexes. In particular, the effect of

[1] To whom correspondence should be addressed.

1090-7807/00 $35.00

having a tensor of rhombic symmetry for the static ZFS was studied. In addition, we discussed the effects of allowing the principal axis system of the static ZFS tensor to deviate from the molecule-fixed frame of the dipole–dipole tensor between the nuclear and electron spins. The influence on the PRE of having a static ZFS of rhombic symmetry was originally recognized by Fukui *et al.* (*24*) for $S = 1$ and $S = 3/2$, and independently by Sharp (*25*) for $S = 1$. The physical interpretation of the rhombicity effect was given by Sharp and co-workers (*25–27*) for $S = 1$, $S = 3/2$, and $S = 2$. The angular effect due to noncoinciding static ZFS and dipole–dipole tensors has been discussed earlier in a paper from our laboratory (*15*) and by others (*25, 26, 28–30*).

In the present paper, the slow-motion theory is generalized to account for complexes of arbitrary electron spin S. Systems with half-integer spin differ physically considerably from those with integer spin, whereas differences among half-integer or integer spins separately are relatively small (*31*). The effect of ZFS rhombicity is for example physically rather different in systems of $S = 1$ and of $S = 3/2$, which we discuss in the present paper. Westlund *et al.* (*14*) extended the slow-motion theory to include arbitrary electron spin; especially, they discussed $S = 3/2$ and $S = 5/2$ systems for the extreme case of a rigid complex (i.e., no transient ZFS was considered). We show NMRD profiles of various illustrative cases for low-symmetry complexes of $S = 3/2$ (e.g., Co^{2+}, Cr^{3+}), where we notice the same type of effects as in paper I, and we discuss the differences from the case of $S = 1$. Although we focus on complexes of $S = 3/2$, a few cases where we vary the electron spin ($S = 1, 3/2, 2, 5/2, 3, 7/2$) are also treated.

There are simplified models beyond the SBM theory that can treat low-symmetry complexes, such as the approach developed by the Florence group of Bertini and co-workers (*4, 29, 32, 33*), which uses the Kubo–Tomita formalism (*34*) and is based on the original work of Lindner (*28*). Very recently, in a project undertaken jointly by us and the Florence group, we made use of the slow-motion calculations as a "benchmark" and improved the Florence model for $S = 1$ systems (*35*) using Redfield theory (*18–22*) to obtain a more accurate description of the electron spin relaxation. In the slow-rotation limit, very good agreement between the two approaches was reached. The concept of *slow rotation,* meaning reorientation much slower than electron spin relaxation, should not be confused with the notion of *slow motion,* meaning that motions responsible for electron spin relaxation (e.g., distortion, vibration, or even reorientation) are not necessarily faster than the electron spin relaxation itself. We also achieved a smooth transition from low to high field in the Florence model, when we implemented the Liouville space superoperator formalism (*16, 17*) for the correlation functions. In the same work, we derived a closed analytical expression for the nuclear spin–lattice relaxation rate in the low-field limit for the case of an axially symmetric static ZFS tensor. Earlier, Westlund had developed a low-field theory (*36*), resulting in a closed analytical expression for $S = 1$, valid in a ZFS-dominated region under the assumption that the static ZFS tensor has rhombic symmetry.

Sharp and co-workers (*25–27, 30, 31, 37–40*) have developed a model very similar to the Florence approach. In all these simplified theories the Redfield limit for the electron spin must be fulfilled, which means that the electron spin relaxation times must not be shorter than the correlation time for the modulation of the relevant interaction causing the relaxation. These approaches are in addition restricted to the slow-rotation condition, because they use the decomposition (DC) approximation (i.e., separate the reorientational motion from the electron spin dynamics). Sharp and co-workers developed a method, based on spin-dynamics simulation (*41*), which is free from the slow-rotation requirement. The most serious problem with all these models (except the modified Florence model for $S = 1$ complexes (*35*)) is, however, that the electron spin relaxation rates are either treated as phenomenological parameters or described using the Bloembergen–Morgan theory (*9*). The slow-motion theory is valid outside of the Redfield limit and for any rate of molecular reorientation.

This paper is organized as follows. In the next section, the generalized slow-motion theory is briefly summarized. In the following section we present and discuss the results, and finally, the conclusions are drawn in the last section.

SLOW-MOTION THEORY

The slow-motion theory is briefly summarized, including the generalization to arbitrary values of S. Westlund has excellently reviewed the slow-motion theory quite recently (*5*), and several other papers describing this subject can be found in the literature (*3, 11–15, 23, 42–46*).

Nuclear Spin Relaxation in Paramagnetic Systems

In general, one assumes that the nuclear spin relaxation is caused by weak coupling to the lattice, which makes the Wangsness–Bloch–Redfield (WBR) theory or simply the Redfield theory (*18–22*) appropriate to use for the nuclear spin system. The electron spin system, on the other hand, is in the slow-motion theory treated together with classical degrees of freedom (reorientation and distortion) as a composite lattice. From the electron spin point of view, the classical degrees of freedom are "seen" as a thermal reservoir. Within the framework of WBR theory, it is the interaction between the nuclear spin system, from which we want to extract information, and the composite lattice, or simply the lattice, that must be put into an explicit form. The PRE of ligand protons in a solution of a paramagnetic transition-metal complex is caused by the modulation of the hyperfine interaction between the nuclear spins and the unpaired electron spins. This hyperfine interaction consists of the through-space dipole–dipole (DD) interaction and the Fermi–contact (or scalar) interaction. Only the DD

interaction is considered in this paper, although the Fermi–contact interaction as well as the contribution of interference between them can be included in the slow-motion theory. The dipole–dipole Hamiltonian is formulated as a contraction of nuclear spin operators, I_n^1, and the lattice operators T_n^1, both operators expressed as standard rank-one irreducible tensor operators (*47*). The components of the lattice operator are written as a scalar contraction of a standard rank-one irreducible spherical tensor operator for the electron spin, with components S_q^1, and the Wigner rotation matrix of rank two (with elements $D^2_{0,n-q}[\Omega_{\mathrm{ML}}(t)]$), which describes the transformation from the molecule-fixed frame (M frame) to the laboratory frame (L frame) through the set of Euler angles Ω_{ML}. The Wigner rotation matrix describes the orientation of the dipole–dipole tensor with respect to the external magnetic field, which defines the direction of the z axis of the laboratory frame. The T_n^1 also contain the electron-nuclear dipole–dipole coupling constant C^{DD} and thus the distance R between the nuclear spin and the paramagnetic center. The relevant equations were given in Paper I.

By using Redfield theory and Liouville space superoperator formalism (*16, 17*) we obtain the expression for the nuclear spin–lattice relaxation rate of ligand nuclei bound to the paramagnetic site as the real part of the complex spectral density taken at the nuclear spin Larmor frequency:

$$T_{1\mathrm{I}}^{-1} = 2\ \mathrm{Re}\{K^{\mathrm{DD}}_{1,1}(-\omega_{\mathrm{I}})\}. \qquad [1]$$

The spectral density in Eq. [1] is given by the Fourier–Laplace transform

$$K^{\mathrm{DD}}_{1,1}(-\omega_I) = \int_0^\infty G^{\mathrm{DD}}_{1,1}(-\tau)e^{-i\omega_{\mathrm{I}}\tau}d\tau, \qquad [2]$$

where the autocorrelation function for the lattice, $G^{\mathrm{DD}}_{1,1}(\tau)$, is given by

$$G^{\mathrm{DD}}_{1,1}(-\tau) = \mathrm{Tr}_{\mathrm{L}}\{T_1^{1\dagger}e^{-i\mathscr{L}_{\mathrm{L}}\tau}T_1^1\rho_{\mathrm{L}}^{\mathrm{eq}}\}. \qquad [3]$$

The autocorrelation function in Eq. [3] contains the lattice operators T_1^1, the lattice density operator (*48*), $\rho_{\mathrm{L}}^{\mathrm{eq}}$, which is assumed to be in thermal equilibrium at all times, and the lattice Liouville superoperator, $\mathscr{L}_{\mathrm{L}}$ (lattice Liouvillian), which determines the time evolution of the system. The expression for the nuclear spin–spin relaxation rate is obtained in the same way (not shown), but includes the spectral density taken at zero frequency as well. We will only consider the case of nuclear spin–lattice relaxation in the present paper. The results obtained this far are very general; in order to come to computationally useful equations we need to specify the lattice dynamics.

The Lattice Dynamics

In the slow-motion theory, the whole lattice is described explicitly, which makes the correlation function in Eq. [3] dependent not only on time but also on orientation. The functional form of the equation of motion for the nuclear spin system now changes from the Redfield equation of motion (includes only time dependence) to the stochastic Liouville equation (includes both time and orientation dependence) (*49–51*). The major advantage of the slow-motion formalism is that it provides a platform for describing electron spin dynamics outside the Redfield limit. The assumption of the pseudorotational modulation of the transient cylindrical ZFS is certainly an oversimplification of a highly complex reality (to get a hint on the ZFS power spectrum from an atomistic description, see the work of Odelius *et al.* (*52, 53*)). However, the pseudorotational model is computationally viable; it hopefully captures essential physics, and it allows meaningful comparison with simpler methods. In the present model the lattice Liouvillian is defined by the terms

$$\mathscr{L}_{\mathrm{L}} = \mathscr{L}_{\mathrm{S}} + \mathscr{L}_{\mathrm{R}} + \mathscr{L}_{\mathrm{D}} + \mathscr{L}^{\mathrm{S}}_{\mathrm{ZFS}} + \mathscr{L}^{\mathrm{T}}_{\mathrm{ZFS}}, \qquad [4]$$

where the first term, $\mathscr{L}_{\mathrm{S}}$, is the Liouville superoperator generated by the electron spin Zeeman Hamiltonian, $H_{\mathrm{S}} = \omega_{\mathrm{S}}S_z$ (the sign of the electron spin Larmor frequency ω_{S} is taken to be the same as that for the magnetogyric ratio γ_{S} by convention). The terms $\mathscr{L}_{\mathrm{R}}$ and $\mathscr{L}_{\mathrm{D}}$ are Markov operators describing the molecular reorientation (R) and distortion (D) of the complex as isotropic rotational and pseudorotational diffusion, respectively. These operators include the characteristic reorientational correlation time τ_{R} and distortional correlation time τ_{D}, both corresponding to rank-two spherical harmonics. The last two terms in Eq. [4] describe the coupling between the electron spin system and the classical degrees of freedom (the thermal reservoir). Both Liouvillians are generated by the corresponding Hamiltonians. Clearly, at any instant, there is only one single ZFS Hamiltonian or Liouvillian. The two terms in Eq. [4] reflect the assumptions that the modulation of the ZFS occurs on two time scales. The term $\mathscr{L}^{\mathrm{S}}_{\mathrm{ZFS}}$ describes the static ZFS interaction, which is averaged over the fast processes (vibrations, collisions) and is subject to rotational modulation. The static ZFS has a strong influence on the energy-level fine structure, especially at low magnetic fields. The term $\mathscr{L}^{\mathrm{T}}_{\mathrm{ZFS}}$ describes the transient ZFS interaction. The transient ZFS has its origin in the distortions of the paramagnetic complex, due to collisions with the surrounding solvent. Its dynamics is modeled as a pseudorotational diffusion. As seen from the molecular frame, the static and transient ZFS represent the mean and the spread, respectively, of the total ZFS (*46*). Under the conditions of slow reorientation, the pseudorotational modulation of the transient ZFS becomes the dominating mechanism for the electron spin relaxation. The static ZFS and the Zeeman interaction which are both modulated by reorientation of the

complex can, if the reorientational motion is sufficiently rapid, affect the electron spin relaxation. This was pointed out in paper I; in addition, Abernathy and Sharp discussed this effect, using spin-dynamics simulation methods, for the cases when reorientation is faster than electron spin relaxation (*41*).

The Hamiltonians of the static and transient ZFS have been given in Paper I. Briefly, both Hamiltonians contain S^2_{-n}, components of a standard rank-two irreducible spherical tensor operator for the electron spin and components of the static and transient ZFS tensor, respectively. In addition, each of the Hamiltonians contains two sets of Wigner rotation matrix elements. One of the sets is common in both operators: $D^2_{m,n}[\Omega_{\mathrm{ML}}(t)]$ describe the transformation from the M to the L frame. The second set of Wigner matrix elements in the static ZFS Hamiltonian, $D^2_{l,m}[\Omega_{\mathrm{P_SM}}]$ describes the transformation from the principal axis system of the static ZFS tensor ($\mathrm{P_S}$ frame) to the M frame. In the transient ZFS Hamiltonian, these are replaced by $D^2_{k,m}[\Omega_{\mathrm{P_TM}}(t)]$, describing the transformation from the principal axis system of the transient ZFS tensor ($\mathrm{P_T}$ frame) to the M frame. The difference between the two sets of Euler angles is that $\Omega_{\mathrm{P_SM}} = (\alpha_{\mathrm{P_S}}, \beta_{\mathrm{P_S}}, 0)$ are treated as time-independent parameters having the simple relation with the spherical polar angles θ and ϕ so that $\alpha_{\mathrm{P_S}} = \phi$ and $\beta_{\mathrm{P_S}} = \theta$. These angles define the orientation of the dipole–dipole tensor with respect to the principal axis system of the static ZFS tensor.

It is customary to define the symmetric and traceless ZFS tensor in terms of the axial (D) and rhombic (E) parameters (*54*). The relations between the irreducible spherical components of the two ZFS tensor and their axial and rhombic parameters can be found in Paper I.

We only consider quadratic terms in the static and transient ZFS Hamiltonians. Thus, we neglect quartic terms that appear for $S > 3/2$ as well as higher-order terms that appear for the lanthanides when $S > 5/2$. These are, anyway, usually very small and are not believed to contribute much to the nuclear spin relaxation compared to the quadratic terms (*9*, *16*), unless the quadratic terms vanish by symmetry. For example, both the axial and rhombic quadratic terms do vanish for complexes of octahedral symmetry, and if the ion has an orbital S state (i.e., $L = 0$) as ground state [e.g., Mn^{2+} ($S = 5/2$)], then the S manifold is split by only quartic terms (*54–56*). In some S state lanthanide complexes (e.g., Gd^{3+} complexes, $S = 7/2$) of octahedral symmetry, quartic as well as sixth-order terms can split the S manifold (*54–56*). Quartic terms can also be important if only the rhombic quadratic term vanishes, which Abernathy *et al.* (*27*) discussed concerning a complex with Mn^{3+} ($S = 2$) of trigonal symmetry.

Energy-Level Splittings for $S \geq 1$

The static ZFS dominates the energy-level fine structure in the low-field limit, and the symmetry of the ligand field at the paramagnetic site influences the splittings. The effects on the energy levels caused by the rhombicity in the static ZFS differ completely between half-integer and integer spin, and this is illustrated in Fig. 1 for the cases of $S = 1$, $3/2$, 2, $5/2$, 3, and 7/2. We have indicated in Fig. 1 some of the splittings in terms of D and E.

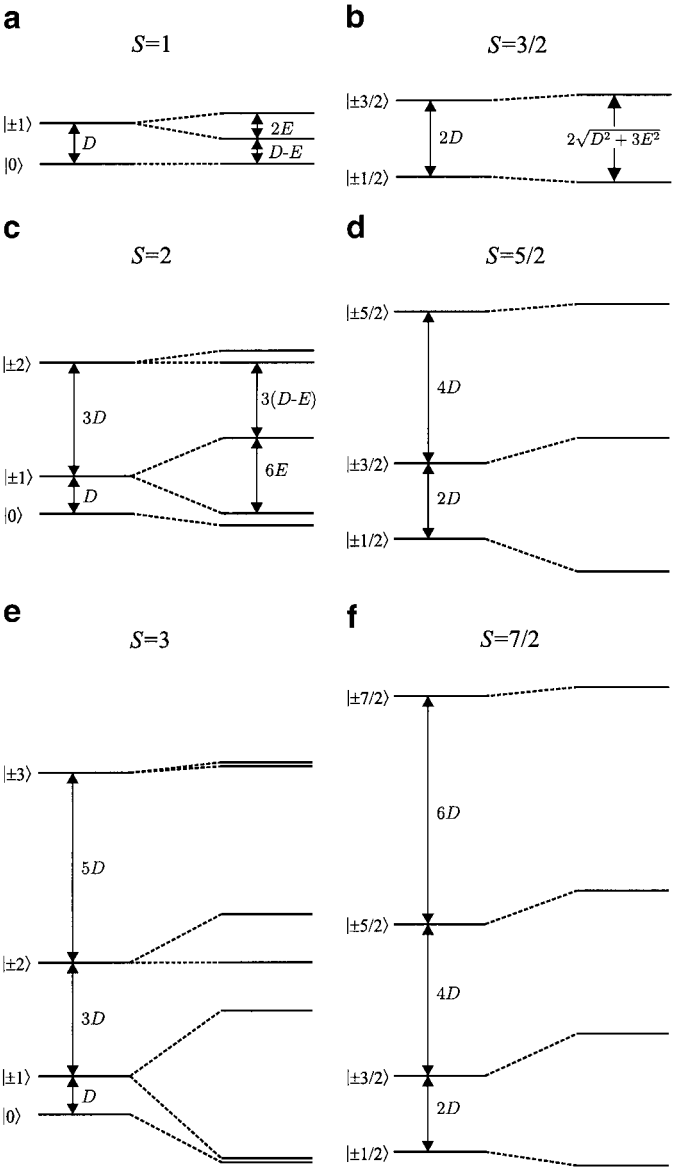

FIG. 1. Energy-level fine structure showing the splitting of the S manifold due to zero-field splitting (ZFS) of axial (left-hand side) and rhombic (right-hand side) symmetry for: (a) $S = 1$, (b) $S = 3/2$, (c) $S = 2$, (d) $S = 5/2$, (e) $S = 3$, and (f) $S = 7/2$. Some of the splittings are given in terms of the ZFS parameters D and E, and the spin states $|M_S\rangle$ as defined in the axial case are displayed on the left-hand side.

In complexes with an axially symmetric ligand field (e.g., D_4 or D_3) for $S = 1$, the energy levels consist of one singlet and one doublet, and the triplet is thus split by the axial component D (left-hand side in Fig. 1a). The degeneracy of the non-Kramers doublet $|\pm 1\rangle$ is split in the first order with $E \neq$

0 for ligand fields of symmetry lower than tetragonal or trigonal, as is shown on the right-hand side in Fig. 1a. This non-Kramers doublet is thus split by $2E$.

For complexes of $S = 3/2$ in a ligand field of axial symmetry, the quartet is split by the axial term in such a way that the energy levels are grouped into two Kramers doublets (left-hand side in Fig. 1b). The Kramers doublets $|\pm\tfrac{1}{2}\rangle$ and $|\pm\tfrac{3}{2}\rangle$ are not split by the rhombic term, independently of the symmetry of the ligand field. This phenomenon, which occurs in all half-integer spin systems, is called the Kramers degeneracy. It is related to time-reversal symmetry and can only be lifted if an external magnetic field is applied (*54–56*). In the low-field limit, only a second-order effect due the rhombic term is generated by making a contribution to the axial splitting between these Kramers doublets, which is illustrated on the right-hand side in Fig. 1b. The Kramers doublets in the case of rhombic symmetry consist of mixed states involving $|\tfrac{1}{2}\rangle$ and $|-\tfrac{3}{2}\rangle$, as well as $|-\tfrac{1}{2}\rangle$ and $|\tfrac{3}{2}\rangle$.

For complexes of $S = 2$ and $S = 3$ in an axially symmetric ligand field, the multiplets are split in the first order by the axial term into one singlet and two ($S = 2$) or three ($S = 3$) non-Kramers doublets, which is shown to the left in Figs. 1c and 1e. The degeneracy of the non-Kramers doublet $|\pm 1\rangle$ is for $S = 2$ split by $6E$. For $S = 3$, the corresponding first-order splitting in a ligand field of rhombic symmetry is $12E$. However, because of the second-order effects, the splitting between the second- and third-lowest energy levels for $S = 3$ is larger than $12E$. The expression for this splitting is rather cumbersome, and therefore we do not show it in Fig. 1e. In fact, for the maximum rhombicity $E/D = 1/3$, the splitting increases by nearly 40%. The degeneracy of the non-Kramers doublet $|\pm 2\rangle$ is for both S-values also lifted in a ligand field of rhombic symmetry, but only in second order, as a result of the different mixing between the $|0\rangle$ and the $|\pm 2\rangle$ states. The splitting due to the rhombic ligand field is shown to the right in Figs. 1c and 1e. A splitting in first order of the non-Kramers doublet $|\pm 2\rangle$ can occur if the quartic term in the static ZFS Hamiltonian is included (not shown), which has been discussed by Sharp and co-workers (*27*).

For complexes of $S = 5/2$ and $S = 7/2$ in a ligand field of axial symmetry, the multiplets are split in the first order by the axial term into three or four Kramers doublets, which is shown to the left in Figs. 1d and 1f. The Kramers doublets are not split in a rhombic ligand field, for the same reason as for $S = 3/2$ (i.e., Kramers degeneracy). The rhombic term produces a second-order contribution to the axial splitting, which is shown to the right in Figs. 1d and 1f.

The impact of the different features when $E \neq 0$ for integer and half-integer spins on the NMRD profiles is discussed in the following section. Note, for example, that the splitting between the two lowest energy levels for $S = 2$ and $S = 3$ becomes rather small if the symmetry of the static ZFS changes from axial to rhombic. This is not the case for $S = 1$, and the difference between these integer spin systems is important for the PRE (see Results and Discussion).

Computational Method

In order to evaluate the spectral density at the nuclear spin Larmor frequency (cf. Eq. [2]), we need to obtain its matrix representation, which is produced by expanding the lattice tensor operators T^1_n in an orthonormal basis set defined in the Liouville space. The Liouville basis set and the projection vectors used in this work are the same as those given in Appendix A of paper I. Once we have set up the supermatrix $\mathbf{M} = i(\mathbf{L}_L + \omega_I\mathbf{1})$ (the matrix elements which are different for the $S > 1$ than for $S = 1$ are given in the Appendix), the computational problem amounts to taking the inverse of it, which yields the expression for the nuclear spin–lattice relaxation rate with arbitrary electron spin S:

$$T_{1I}^{-1} = \tfrac{4}{3}(C^{DD})^2 S(S+1)\mathrm{Re}\{\mathbf{c}_1^*\mathbf{M}^{-1}\mathbf{c}_1\}. \qquad [5]$$

Because the projection vectors $\mathbf{c}_1$ only contain three non-zero elements for the DD interaction (see paper I), a 3×3 fragment of the inverse supermatrix $\mathbf{M}^{-1}$ is sufficient. The supermatrix $\mathbf{M}$ is sparse, and the size of it, which in principle is infinitely large due to the classical degrees of freedom, depends on the convergence properties in the inversion routine. The inversion of $\mathbf{M}$ is performed numerically by means of the Lanczos algorithm (*57*). The size of the supermatrix is increased step by step until convergence of the desired accuracy is accomplished.

The dimension of the supermatrix for $S = 3/2$ is much larger than for $S = 1$, mostly due to the increase of the spin space. For systems with $S = 1$, the dimension was about $10{,}000 \times 10{,}000$ at the most (see paper I), but for systems with $S = 3/2$ a dimension of about $40{,}000 \times 40{,}000$ is necessary in order to reach convergence (these values correspond to the most general situation when $\theta \neq 0$). The principal quantum numbers A and L of the basis operators (see Paper I), corresponding to the isotropic pseudorotational diffusion and the rotational diffusion, respectively, determine the dimension, together with the electron spin part. The dimension for $S = 3/2$, which we mentioned above, corresponds to $A = 4$ and $L = 12$, whereas for $S = 1$ the values $A = 4$ and $L = 8$ have been used. The number of non-zero matrix elements, which is the real factor that determines the speed of the program, increases from about 400 thousand for $S = 1$ to approximately four million for $S = 3/2$ when $\theta \neq 0$. In Table 1 we have collected the dimension (denoted DIM), the number of non-zero matrix elements (denoted NEL) for the case when $\theta \neq 0$, and the corresponding values of the principal quantum numbers (A and L) for $S = 1$, 3/2, 2, 5/2, 3, and 7/2 in the case of large static ZFS ($\Delta_S = 10\ \mathrm{cm}^{-1}$). For small static ZFS, a smaller value of L may suffice, which reduces the dimension. Moreover, the value of NEL is reduced if $\theta = 0$. It is clear from

TABLE 1

Dimension of the Supermatrix (DIM), Number of Non-zero Matrix Elements (NEL), and Corresponding Values of A and L for Various S under the Condition of Large Static ZFS ($\Delta_S = 10\ cm^{-1}$) and for $\theta \neq 0$

S	A	L	DIM	NEL
1	4	8	10,000	4×10^5
3/2	4	12	40,000	4×10^6
2	4	12	60,000	7×10^6
5/2	4	12	90,000	1×10^7
3	4	12	120,000	2×10^7
7/2	4	12	150,000	3×10^7

Table 1 that, as the spin system increases, the dimensions increase markedly. For the convergence tests and most of the production computation of the NMRD profiles, we have used parallel computers (IBM SP2). Only in some cases was it possible to use an ordinary PC (two 180 MHz Pentium processors) with extended RAM memory (512 MByte).

RESULTS AND DISCUSSION

The results presented in this section refer to the nuclear spin relaxation rate in the paramagnetic complex. We assume fast-exchange conditions (*1*, *2*) and neglect the outer-sphere relaxation (the influence of the paramagnetic ion on the relaxation of water protons outside of its first coordination sphere). Under these conditions, the measured ligand proton relaxation rates and the relaxation rate in the paramagnetic complex are given as

$$T_1^{-1}(\text{para}) - T_1^{-1}(\text{dia}) = T_{1,P}^{-1} = P_M q T_{1I}^{-1}, \qquad [6]$$

where T_1^{-1}(para) is the relaxation rate of the ligand proton in a paramagnetic solution, T_1^{-1}(dia) is the corresponding rate in a diamagnetic solution, and $T_{1,P}^{-1}$ is the PRE. P_M is the mole fraction of the transition-metal complex, and q is the coordination number (i.e., number of ligand molecules in the complex). Since the product $P_M q$ is just a constant, we may arbitrary set it equal to 10^{-3} to obtain the PRE in units of ms^{-1}. In this particular case we call T_{1I}^{-1} for PRE, which is displayed as a function of the magnetic field in the NMRD profiles.

In this section we present a large number of calculated NMRD profiles which illustrate various types of systems with respect to symmetry and deformability. Some of the parameters are held fixed throughout all cases, at the values used in Paper I for Ni(II), $S = 1$ systems. For the nuclear spin–electron spin distance, R, the value 255 pm is used. For the correlation times, τ_D (corresponding to the distortional motion), we use the value 4 ps, while τ_R (corresponding to the reorientational motion) is assigned a value of 60 ps. The electronic g-factor is set to 2.25 and is assumed to be isotropic. The azimuthal angle ϕ is set to zero in all cases (according to test calculations, the effects of varying that angle are rather small). The polar angle θ has profound effects in $S = 1$ systems (see paper I) when we vary it between the values 0°, 45°, and 90°, and this is discussed also for $S = 3/2$ systems. The square of the magnitude of the static ZFS, Δ_S, is defined as the sum of the squared diagonal components of the static ZFS tensor, for which we use the values 1 and 10 cm^{-1}. The relation between Δ_S and the tensor components D_S and E_S is $\Delta_S^2 = \frac{2}{3}D_S^2 + 2E_S^2$. For the ratio E_S/D_S we use the values 0, 0.1, and $\frac{1}{3}$ (the maximum possible) so as to keep the magnitude constant. For Δ_S equal to 1 and 10 cm^{-1} we have $\omega_{\Delta_S}\tau_R$ equal to 11 and 110, respectively (ω_{Δ_S} corresponds to Δ_S but in units of rad/s), and from this we can immediately see that we are outside of the strong narrowing condition, or Redfield limit (corresponding to $\omega_{\Delta_S}\tau_R \ll 1$) with respect to the static ZFS. The magnitude of the transient ZFS, Δ_T, is defined in analogy with the static ZFS. Since we concentrate on the cylindrically symmetric transient ZFS, we have here the relation $\Delta_T^2 = \frac{2}{3}D_T^2$. We use the values 0.5 and 10 cm^{-1} for the magnitude Δ_T in all cases. For Δ_T equal to 0.5 and 10 cm^{-1} we have $\omega_{\Delta_T}\tau_D$ equal to 0.4 and 8, respectively. From this we see that the former case is within the Redfield limit (corresponding to $\omega_{\Delta_T}\tau_D \ll 1$), and the latter is in the slow-motion regime with respect to the transient ZFS.

We use the same terminology as in paper I, where the physical interpretation is given in terms of the different parameters: *slightly asymmetric complex* when $\Delta_S = 1\ cm^{-1}$; *asymmetric complex* when $\Delta_S = 10\ cm^{-1}$; *weakly deformable complex* when $\Delta_T = 0.5\ cm^{-1}$; *highly deformable complex* when $\Delta_T = 10\ cm^{-1}$; *no rhombicity* when $E_S/D_S = 0$; *intermediate rhombicity* when $E_S/D_S = 0.1$; *large rhombicity* when $E_S/D_S = \frac{1}{3}$; *coinciding axes* when $\theta = 0$ and $\phi = 0$.

We now turn to the discussion of a series of different cases. In the first two sections we show the effects on the NMRD profiles when we vary the parameters Δ_S, E_S/D_S, Δ_T, and θ for $S = 3/2$. One of the sections deals with cases corresponding to the Redfield limit with respect to the transient ZFS (i.e., $\Delta_T = 0.5\ cm^{-1}$). In the other section we cover a selection of cases within the slow-motion regime (i.e., $\Delta_T = 10\ cm^{-1}$). We should point out that in paper I we showed NMRD profiles for $S = 1$ near the Redfield limit, which corresponds to $\Delta_T = 1\ cm^{-1}$. The corresponding NMRD profiles in the case of $S = 3/2$, however, have characteristics very similar to those within the Redfield limit. Thus, we choose not to show or discuss them. In the next section we discuss the features in the NMRD profiles due to different values of the electron spin ($S = 1$, 3/2, 2, 5/2, 3, and 7/2). We also show in the first section (i.e., within the Redfield limit) the calculated NMRD profile corresponding to the SBM theory using the same parameter values as those used in the slow-motion calculations (note, however, that the static ZFS is absent in the SBM theory). In addition, we have also tried to fit the SBM theory to two of the slow-motion profiles (the curves corresponding to D_S values of 1 and 10 cm^{-1} and no rhombicity).

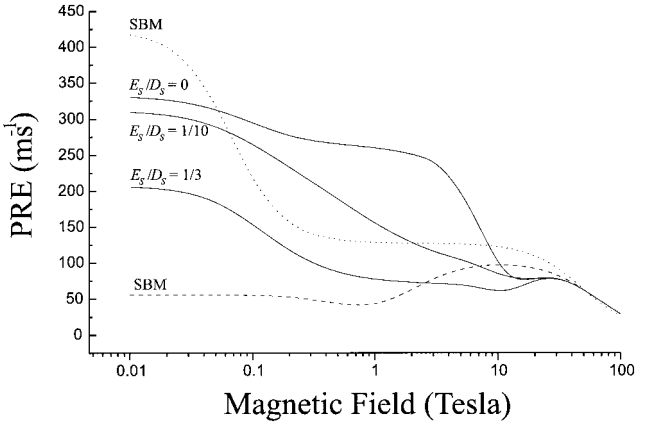

FIG. 2. NMRD profiles for asymmetric ($\Delta_S = 10\ cm^{-1}$), weakly deformable ($\Delta_T = 0.5\ cm^{-1}$) complexes of $S = 3/2$ with increasing rhombicity in the static ZFS (E_S/D_S) at the angle $\theta = 0°$. No rhombicity in the transient ZFS ($E_T/D_T = 0$) and $\phi = 0°$. The dashed curve corresponds to the SBM theory using the same parameters as for the slow-motion calculations, except that static ZFS is absent. The dotted curve corresponds to a fitting of the SBM theory to the slow-motion profile where $E_S/D_S = 0$ (obtained best-fit parameters are given in Table 2).

Before moving on to the examples, we wish to provide a qualitative picture of the field-dependence of the PRE. In qualitative terms, the shape of a NMRD profile can be considered to arise from a series of Lorentzian curves, characterized by different "correlation times" and frequencies. The frequencies are related to the energy level structure. The "correlation times" are influenced (sometimes even dominated) by electron spin relaxation and can be field-dependent. In the presence of static ZFS, we do not expect any field-dependence of the PRE at very low fields (weak Zeeman interaction): the changes of the characteristic frequencies and "correlation times" of the system with the magnetic field are negligible. When the field increases and the product of a "correlation time" with the corresponding frequency becomes close to unity, the Lorentzian disperses and there is a decrease in the NMRD profile. A rise in the NMRD profiles can take place if the "correlation time" increases, which normally occurs because the electron spin relaxation slows down at high field.

Cases for S = 3/2 within the Redfield Limit ($\Delta_T = 0.5\ cm^{-1}$)

Asymmetric and weakly deformable complexes. The NMRD profiles in Fig. 2 (solid lines) show the effect of increasing the rhombicity in the static ZFS when the angle θ is zero for the case of asymmetric (large static ZFS), weakly deformable (small transient ZFS) complexes.

The first feature that we wish to point out as distinguishing the $S = 3/2$ systems from $S = 1$ is the occurrence of a "double plateau" in the low-field regime in the absence of rhombicity. This "double plateau" structure was noticed by Westlund *et al.* (*14*) in their work on half-integer spins in rigid complexes. It was then assigned to lifting the degeneracy in the $|\pm\frac{1}{2}\rangle$ Kramers doublet by ω_S when the external magnetic field increases. The second important feature, different in the case of $S = 3/2$ and $S = 1$ systems, concerns the rhombicity effect. Increasing the rhombicity in Fig. 2 has the effect of reducing the PRE substantially in the low-field region (less than about 10 Tesla), but not as drastically as for $S = 1$ complexes (cf. paper I), where the rhombicity effect completely quenches the dipole–dipole coupling and reduces the PRE practically to zero. The reason for the smaller effect in the $S = 3/2$ case is that the rhombic term in the static ZFS Hamiltonian only affects the axial splitting between the Kramers doublets in second order, and the Kramers doublets themselves remain degenerate (see Fig. 1). We can also see that the rhombicity affects the two plateaus in a somewhat different way. The region to the right of the first plateau (about 0.1–10 Tesla) is more sensitive to the rhombicity effect than the region to the left. We have the following explanation of this observation. We can recall from the work on $S = 1$ that the drastic effect of the rhombicity could be explained by the suppression of the unique quantization axis and the permanent magnetic moment of the electron in the rhombic case. The situation for $S = 3/2$ is in this respect more complicated. The quantization of the electron spin within the $|\pm\frac{1}{2}\rangle$ levels differs considerably from that within the $|\pm\frac{3}{2}\rangle$ levels (*27*). In the former case the quantization axis is oriented in the direction of the external magnetic field, which means that a quantization axis can still be defined irrespective of the symmetry of the static ZFS, which is different from the $S = 1$ case (cf. paper I). The quantization in the $|\pm\frac{3}{2}\rangle$ subsystem behaves in the same way as for integer spins, which means that the quantization axis is defined in the molecule-fixed P_S frame only for axially symmetric complexes. Now, in the rhombic case the states within one Kramers doublet are mixed with those of the other Kramers doublet. This means that the electron spin Zeeman interaction affects the axial splitting, which gives rise to a different field dependence of the PRE when $E_S \neq 0$ than when $E_S = 0$.

For comparison purposes, we also show in Fig. 2 (dashed line) the calculated profile corresponding to the SBM theory using the same parameter values as for the slow-motion calculations, but without static ZFS since it is not included within the SBM theory. The difference in the profiles between the SBM and slow-motion theories is striking. The main reason for the poor agreement is that static ZFS has a very large impact on the electron spin relaxation, which is not taken into account within the SBM theory. This effect is discussed in another paper by us (*58*), where a low-field limiting theory in closed analytical form for high-spin systems has been developed. The dotted curve in Fig. 2 corresponds to a fitting of the SBM theory to the slow-motion profile where $E_S/D_S = 0$. Clearly, the SBM theory is not even close in predicting the functional form of the slow-motion profile, and the best-fit parameters, which are given in Table 2, are badly off.

The NMRD profiles in Fig. 3 show the effect of increasing the angle θ when the rhombicity in the static ZFS is zero for the

TABLE 2

Nonlinear Least-Squares Fitting of the SBM Theory to the Calculated NMRD Profiles Obtained Using the Slow-Motion Theory in Figs. 2 and 4 ($\Delta_S = 10$ cm^{-1} and $\Delta_S = 1$ cm^{-1}, Respectively) for $E_S/D_S = 0$

		SBM	
	Slow-motion	$\Delta_S = 10$ cm^{-1}	$\Delta_S = 1$ cm^{-1}
R (pm)	255	256	252
τ_R (ps)	60	76	52
τ_D (ps)	4	1.3×10^{-5}	2.6
Δ_T (cm^{-1})	0.5	0.51×10^{-3}	0.34
σ	—	0.30398	0.09915

Note. The symbol σ is the relative standard deviation of the fit.

case of asymmetric (large static ZFS), weakly deformable (small transient ZFS) complexes.

Increasing the angle θ reduces the PRE in the low-field region in the same way as for systems of $S = 1$ (cf. paper I). The reduction in the PRE is about the same in the whole low-field region and thus shows different characteristics in the NMRD profile than the rhombicity effect does (cf. Fig. 2). This distinction is not very pronounced in the case of $S = 1$ (see paper I), because for integer spin systems the sensitivity to the rhombicity effect is the same over the whole low-field region, as opposed to what we discussed for $S = 3/2$ above. The sensitivity to the angular effect is of course also the same over the whole low-field region, since we can regard this feature as a scaling of the dipole–dipole coupling strength. For a certain range of stronger magnetic fields (about 10–20 Tesla) the same trend as for $S = 1$ is present, namely, that the curve with largest value of the PRE is that for $\theta = 45°$ (cf. paper I).

Increasing the angle θ when $E_S \neq 0$ (not shown) does not reveal any new features, but reduces the PRE in the same way as in Fig. 3. We have also tested the dependence of the PRE on the angle θ for the case of large, rhombic static ZFS and small transient ZFS. The variation of the PRE with that angle was

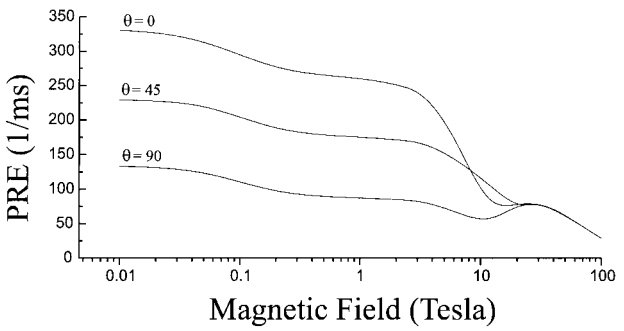

FIG. 3. NMRD profiles for asymmetric ($\Delta_S = 10$ cm^{-1}), weakly deformable ($\Delta_T = 0.5$ cm^{-1}) complexes of $S = 3/2$ with increasing angle θ (in degrees) at the rhombicity $E_S/D_S = 0$. No rhombicity in the transient ZFS ($E_T/D_T = 0$) and $\phi = 0°$.

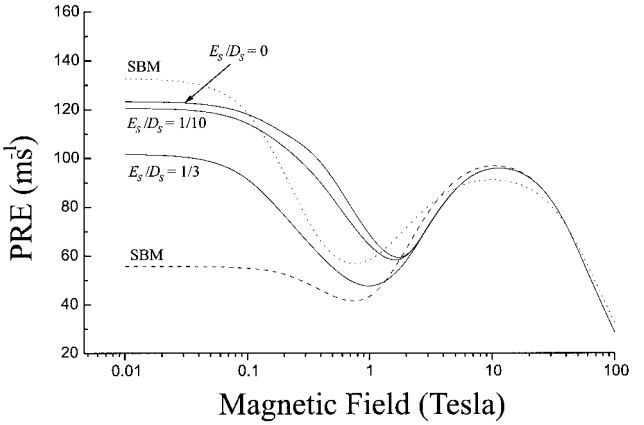

FIG. 4. NMRD profiles for slightly asymmetric ($\Delta_S = 1$ cm^{-1}), weakly deformable ($\Delta_T = 0.5$ cm^{-1}) complexes of $S = 3/2$ with increasing rhombicity in the static ZFS (E_S/D_S) at the angle $\theta = 0°$. No rhombicity in the transient ZFS ($E_T/D_T = 0$) and $\phi = 0°$. The dashed curve corresponds to the SBM theory using the same parameters as for the slow-motion calculations, except that static ZFS is absent. The dotted curve corresponds to a fitting of the SBM theory to the slow-motion profile where $E_S/D_S = 0$ (obtained best-fit parameters are given in Table 2).

limited and is not shown. In the remainder of this section we will only discuss the effect of the angle θ for $E_S = 0$.

Slightly asymmetric and weakly deformable complexes. The NMRD profiles in Fig. 4 (solid lines) show the effect of increasing the rhombicity in the static ZFS when the angle θ is zero for the case of slightly asymmetric (small static ZFS), weakly deformable (small transient ZFS) complexes.

The NMRD profiles in Fig. 4 are rather different from those in Fig. 2, where the magnitude of the static ZFS is 10 times larger. First, the dispersion in Fig. 2 at about 10 Tesla is shifted to about 1 Tesla in Fig. 4, with the consequence that the first dispersion and the second plateau (both counted from the left), which were clearly distinguished in Fig. 2, are practically absent in Fig. 4. In fact, the two dispersions shown in Fig. 4 are almost superimposed on each other, resulting in one rather flat dispersion. Another interesting difference between the curves in Fig. 4 and those in Fig. 2 is the large reduction in the PRE (more than 60%) at very low magnetic fields for the low Δ_S compared to the high Δ_S. This is also very different compared to $S = 1$ systems (see paper I), where the PRE values were practically the same at low fields for Δ_S values of 1 and 10 cm^{-1}. However, a small maximum appeared just before the dispersion for the larger value of the static ZFS in the case of $S = 1$, which is not present in $S = 3/2$ systems. We tentatively explain these differences between $S = 1$ and $S = 3/2$ systems by differences in the field dependence of electron spin relaxation. A more thorough analysis of the differences in electron spin relaxation effects is discussed in another paper by us (*58*) on a novel low-field, Redfield-limit theory of PRE.

Increasing the rhombicity has the effect of reducing the PRE at low magnetic fields, but not at all as much as in Fig. 2. This is so especially in the region just to the left of the dispersion,

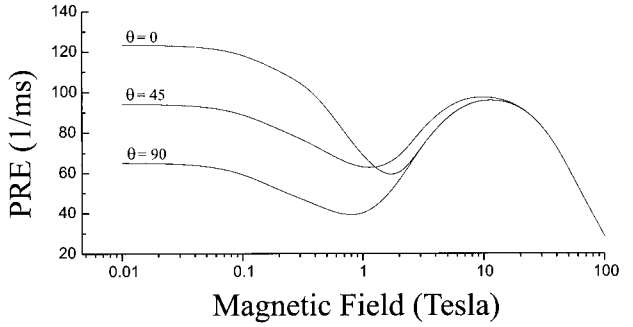

FIG. 5. NMRD profiles for slightly asymmetric ($\Delta_S = 1$ cm^{-1}), weakly deformable ($\Delta_T = 0.5$ cm^{-1}) complexes of $S = 3/2$ with increasing angle θ (in degrees) at the rhombicity $E_S/D_S = 0$. No rhombicity in the transient ZFS ($E_T/D_T = 0$) and $\phi = 0°$.

which was particularly sensitive to the rhombicity for large static ZFS. The reason is the same as that discussed above, namely, that the second plateau is absent because the second dispersion is shifted to the left.

The profile in Fig. 4 corresponding to the SBM theory (dashed line) agrees poorly with the slow-motion profile even for a smaller value of the static ZFS parameter D_S (here, 1 cm^{-1} as compared to 10 cm^{-1} used in the curves in Fig. 2). Note that the SBM curves in Figs. 2 and 4 are the same since the only difference in the parameter values is related to a change in the magnitude of the static ZFS. The fitting of the SBM theory to the slow-motion profile ($E_S/D_S = 0$) improves somewhat compared to that for a larger value of D_S in Fig. 2, but the shape of the curve (dotted line in Fig. 4) and the best-fit parameter values (see Table 2) are still rather different from the profile and parameter values corresponding to the slow-motion theory.

The NMRD profiles in Fig. 5 show the effect of increasing the angle θ when the rhombicity in the static ZFS is zero for the case of slightly asymmetric (small static ZFS), weakly deformable (small transient ZFS) complexes.

Increasing the angle θ reduces the PRE to about the same extent as for large static ZFS, as shown in Fig. 3. The range of magnetic fields where the value of PRE is the largest for $\theta = 45°$ has increased compared with Fig. 3. In Fig. 5 it ranges from about 1 to 20 Tesla, whereas in Fig. 3 the range was about 10–20 Tesla. In $S = 1$ systems the opposite trend is true: the case of large static ZFS has the widest range of magnetic fields where the NMRD profile for $\theta = 45°$ is above the $\theta = 0°$ profile (cf. paper I). The physical reason for this difference between the $S = 3/2$ and $S = 1$ systems is also here tentatively related to the difference in electron spin relaxation and its variation with transition frequencies as Δ_S changes.

Cases for $S = 3/2$ within the Slow-Motion Regime ($\Delta_T = 10$ cm^{-1})

Asymmetric and highly deformable complexes. We now discuss complexes with large magnitudes of the transient ZFS, which correspond to slow-motion cases. In the slow-motion regime the electron spin lineshapes are combinations of infinitely many Lorentzians, with the consequence that we are faced with a broad spectrum of electron spin relaxation times. This feature, which we will refer to as the *slow-motion effect*, results in very rapid "effective" electron spin relaxation. It should be stressed that NMRD profiles in the slow-motion regime showing the effects due to either the variation in the rhombicity in the static ZFS or the variation of the angle θ have never been treated before, and they cannot be handled by simple theories such as the SBM theory, the Florence model, or the approach by Sharp.

The NMRD profiles in Fig. 6 show the effect of increasing the rhombicity in the static ZFS when the angle θ is zero for the case of asymmetric (large static ZRS), highly deformable (large transient ZFS) complexes.

Increasing the rhombicity reduces the PRE, but not as markedly as for a small magnitude of the transient ZFS (cf. Fig. 2). However, compared to $S = 1$ systems, which are practically independent of the rhombicity in the static ZFS in the slow-motion regime, the change in PRE in $S = 3/2$ systems is not negligible.

The NMRD profiles in Fig. 7 show the effect of increasing the angle θ when the rhombicity in the static ZFS is zero for the case of asymmetric (large static ZFS), highly deformable (large transient ZFS) complexes.

Increasing the angle θ reduces the PRE very much in the same way as in Fig. 3, but not to the same extent. Analogous to the rhombicity effect in Fig. 6, the PRE is much more sensitive to a change in the angle θ for $S = 3/2$ complexes than for those with $S = 1$, in which it is almost θ-independent. The physical reason for the differences between the $S = 3/2$ and $S = 1$ cases, concerning both the θ dependence and the rhombicity effect in the static ZFS, is related to the slow-motion effect. Thus, the "effective" electron spin relaxation is much more rapid in $S = 1$ than in $S = 3/2$ systems, because of the Kramers degeneracy in the latter.

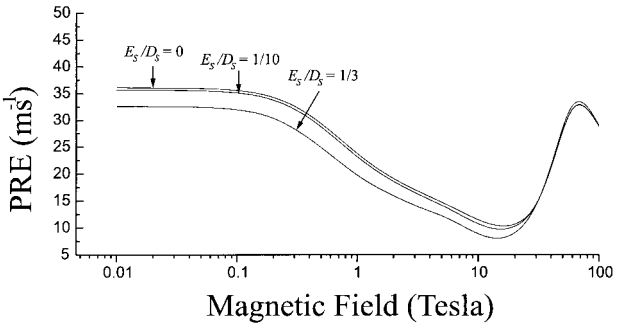

FIG. 6. NMRD profiles for asymmetric ($\Delta_S = 10$ cm^{-1}), highly deformable ($\Delta_T = 10$ cm^{-1}) complexes of $S = 3/2$ with increasing rhombicity in the static ZFS (E_S/D_S) at the angle $\theta = 0°$. No rhombicity in the transient ZFS ($E_T/D_T = 0$) and $\phi = 0°$.

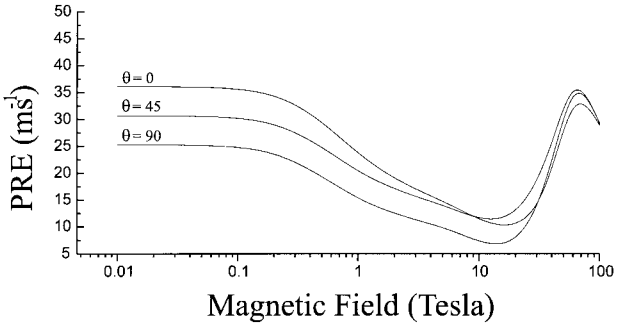

FIG. 7. NMRD profiles for asymmetric ($\Delta_S = 10$ cm^{-1}), highly deformable ($\Delta_T = 10$ cm^{-1}) complexes of $S = 3/2$ with increasing angle θ (in degrees) at the rhombicity $E_S/D_S = 0$. No rhombicity in the transient ZFS ($E_T/D_T = 0$) and $\phi = 0°$.

The effect on the PRE of changing either the rhombicity in the static ZFS or the polar angle θ for a small Δ_S is negligible; therefore we do not show any NMRD profiles for these cases. The PRE is particularly insensitive to the rhombicity effect where the curves of different E_S/D_S (not shown) coincide. We noted similar features for $S = 1$ in paper I. The following physical picture of this phenomenon can be invoked. Since the transient ZFS momentarily dominates over the static ZFS, the energy-level structure can at each instant be considered as being determined by the transient rather than the static part. In this picture, the rhombicity in the static ZFS is not expected to significantly affect the PRE.

Comparison of Different Electron Spins (S = 1, 3/2, 2, 5/2, 3, and 7/2)

In this section, we discuss the differences between complexes of different S values, something which has been done earlier by Sharp for some cases under slow-rotation conditions (*31*). Here we study cases of more rapid reorientation and also extend the analysis to cover cases with a static ZFS of rhombic symmetry. In another paper by Sharp and co-workers (*27*), they did in fact discuss the rhombicity effect for different S values briefly, but this was again for slowly rotating complexes, and they did not show any NMRD profiles illustrating this feature. In order to compare the characteristics in the NMRD profiles for different S in a proper way, we use a reduced spectral density (RSD) $\tilde{K}^{DD}_{1,1}(-\omega_I)$, which we define in the following way:

$$\tilde{K}^{DD}_{1,1}(-\omega_I) = \frac{T_{1I}^{-1}}{(4/3)(C^{DD})^2 S(S+1)\tau_R}. \qquad [7]$$

The division by $S(S + 1)$ in Eq. [7] means that the same factor included in T_{1I}^{-1} (cf. Eq. [5]) will cancel; thus, only differences inherent in the electron spin system (e.g., relaxation and energy-level effects) for various S are shown in the profiles. The maximum value the RSD can attain at low field is unity, when the electron relaxation effects are absent and the only modulation of the DD interaction originates from the complex reorientation.

The NMRD profiles in Fig. 8 show the effect of increasing the electron spin S for the case of slightly asymmetric (small static ZFS), weakly deformable (small transient ZFS) complexes when the symmetry of the static ZFS is axial (Fig. 8a) and rhombic (Fig. 8b), and for coinciding axes ($\theta = \phi = 0$).

If we compare the NMRD profiles in Fig. 8a of integer spin pairwise with those of half-integer spin, $S = 1$ with $S = 3/2$, $S = 2$ with $S = 5/2$, and $S = 3$ with $S = 7/2$, we see that the low-field plateaus for half-integer spins are higher except in the last case, for which the low-field plateaus coincide. We note that, with the particular choice of parameters at hand, the rapid electron spin relaxation phenomena reduce the efficiency of the PRE at low field by about 65% for $S = 3/2$ compared to about 75% for the highest spins. The details of these electron spin relaxation effects on the PRE will be elaborated in the forthcoming work on the low-field, Redfield-limit theory (*58*). Here, we only note that in the simple BM approach the electron spin relaxation rates are expected to increase monotonously with increasing S. This clearly shows that this Zeeman-limit theory is not appropriate for the analysis of high-spin systems in the ZFS-dominated regime. The order of the low-field plateaus within the integer and half-integer spin systems is the same; that is, the plateau is reduced when S increases. How-

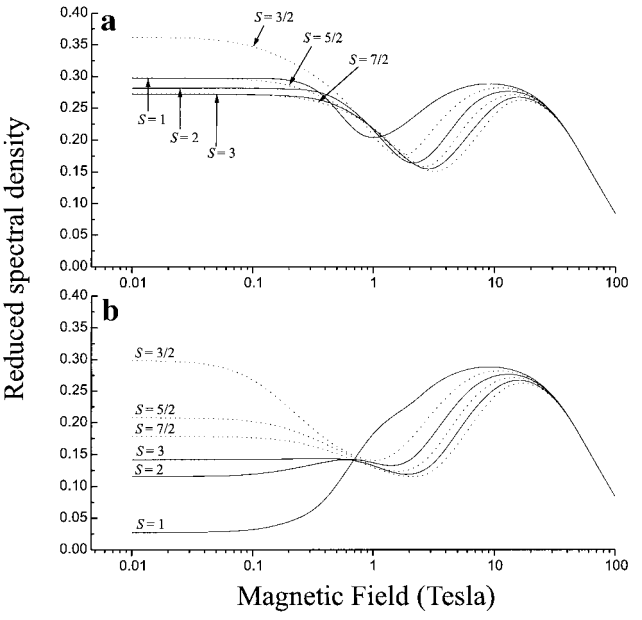

FIG. 8. NMRD profiles for slightly asymmetric ($\Delta_S = 1$ cm^{-1}), weakly deformable ($\Delta_T = 0.5$ cm^{-1}) complexes with increasing electron spin S at (a) no rhombicity in the static ZFS ($E_S/D_S = 0$), and (b) with rhombicity in the static ZFS ($E_S/D_S = 1/3$). The angle $\theta = 0°$ and $\phi = 0°$. Reduced spectral densities have been used rather than PRE in order to compare NMRD profiles of different S. Curves with integer spin are displayed as solid lines, whereas those of half-integer spin are shown as dotted lines.

ever, the reduction of the PRE is larger in the case of half-integer spin systems than in the case of integer spin systems.

In Fig. 8b we show NMRD profiles for various S in the case of a rhombic static ZFS ($E_S/D_S = 1/3$). The RSDs are reduced in the low-field region for all spin systems compared to the case of an axial static ZFS (cf. Fig. 8a). The RSD for integer S are reduced more drastically than for half-integer spin systems, because of the Kramers degeneracy in the latter. We discussed this phenomenon in a previous section in the case of $S = 3/2$ for electron spin relaxation within the Redfield limit, and it applies to all half-integer spin systems. The order of the low-field plateaus of the half-integer spin systems in the rhombic case remains the same as in the axial case (cf. Figs. 8a and 8b). However, for the integer spin systems the order is reversed; that is, $S = 1$ has the lowest PRE and $S = 3$ the highest. The explanation for this is related to the splitting of the two lowest energy levels (see Figs. 1a, 1b, and 1c). This splitting becomes rather small for $S = 2$ and $S = 3$ in the case of a rhombic as compared to an axial static ZFS. This reduction in the splitting is not as dramatic in the case of $S = 1$. Increasing this splitting will produce a reduction in the RSD in a similar way as for the splitting of the non-Kramers doublet $|\pm 1\rangle$. Thus, since the splitting increases in going from $S = 3$ to $S = 1$, the RSD will be reduced, which is seen in Fig. 8b.

CONCLUSIONS

We have shown NMRD profiles where we can investigate the effect on the PRE of symmetry-breaking properties, in particular for $S = 3/2$. We have discussed the differences between $S = 3/2$ and $S = 1$ systems concerning these effects. We find that the rhombicity effect in the static ZFS reduces the PRE substantially, but not as drastically as for $S = 1$ complexes, due to the Kramers degeneracy in $S = 3/2$ systems. The consequence of the Kramers degeneracy is that the rhombic term E_S only produces a second-order contribution to the axial splitting, which in turn provides $S = 3/2$ complexes with a slower electron spin relaxation than for $S = 1$. We have also seen that NMRD profiles are sensitive to the rhombicity effect also in the slow-motion regime, which was not the case for $S = 1$ (see paper I). The effect of changing the angle θ is rather similar for $S = 3/2$ and $S = 1$ complexes, except in the slow-motion regime where the former show a larger change in the PRE.

NMRD profiles corresponding to the SBM theory have also been shown and compared with the slow-motion profiles and the disagreement is very pronounced. Even if we fit the SBM theory to the calculated slow-motion curves the fitted curves do not have the same functional form as those based on the slow-motion theory. In addition, the best-fit parameter values differ substantially from those used in the slow-motion calculation. Clearly, the SBM theory cannot mimic the low and intermediate magnetic field parts of the NMRD profiles for low-symmetry complexes when static ZFS is present. The main reason for this is that the BM theory breaks down because the strong influence of the static ZFS on the electron spin relaxation is not taken into account (see the other paper by us (*58*)).

We have also investigated the effect on the PRE, or rather on the RSD, of changing the electron spin S. We have found that integer spin systems behave differently than half-integer systems, due to the Kramers degeneracy in the latter, which is in agreement with what Sharp has discussed in earlier papers (*27, 31*). The order of the low-field plateaus in the case of an axial static ZFS is the same for integer as for half-integer spin systems; that is, the RSD is reduced as S increases. Sharp predicted a somewhat more pronounced distinction between integer and half-integer spin systems in the axial case. The value for Δ_S that we have chosen (1 cm^{-1}) in Fig. 8 only displays a pronounced distinction between $S = 3/2$ and the other spin quantum numbers. If we had chosen a larger values of Δ_S, then the profiles of the half-integer spin systems would have been grouped together on a somewhat higher level than those with integer spin. Clearly, the ordering of the low-field plateaus depends strongly on the magnitude of the static ZFS, which we tentatively trace to the electron spin relaxation properties of $S > 1$ systems.

In the case of a rhombic static ZFS, the order of the low-field plateaus for integer spin systems is reversed compared to the axial case. This phenomenon is related to the splitting between the two lowest energy levels, which increases as S decreases and hence produces a smaller value of the RSD. For half-integer spin systems the order of the low-field plateaus remains the same if the symmetry in the static ZFS is changed.

The present paper, together with paper I, provides a wide range of cases of calculated NMRD profiles covering features of integer spin, with $S = 1$ as an example (paper I), and now also half-integer spin, exemplified with $S = 3/2$. Some cases of $S > 3/2$ are also discussed in the present paper. Although this set of NMRD profiles is not complete, it covers practically most of the cases where zero-field splitting is dominating. Simplified models may be tested against these NMRD profiles and may be modified accordingly. One example of this strategy is the successful cooperation between the authors and the Florence group that resulted in an improved version of the Florence model with very good agreement in the slow-rotation limit for the case of $S = 1$ (*35*).

APPENDIX: SUPERMATRIX ELEMENTS

The supermatrix elements of the static and transient ZFS Liouvillians, $\mathcal{L}^S_{ZFS}$ and $\mathcal{L}^S_{ZFS}$, are given here, using the orthonormal basis operators defined in Appendix A of paper I. These supermatrix elements are valid for an arbitrary value of S, whereas those in paper I were restricted to the case of $S = 1$. The supermatrix elements of the other superoperators contained in the lattice Liouvillian $\mathcal{L}_L$ are exactly the same as

those given in Appendix B in paper I and are therefore not given here.

$$
\begin{aligned}
&(A'B'C'|(L'K'M'|(\Sigma'\sigma'|\mathcal{L}^{\mathrm{S}}_{\mathrm{ZFS}}|\Sigma\sigma)|LKM)|ABC) \\
&\quad = \delta_{A'A}\delta_{B'B}\delta_{C'C}(-1)^{\sigma+K'-M'} \times \sqrt{5}((-1)^{\Sigma'+2+\Sigma}-1) \\
&\qquad \times \sqrt{\frac{(2L'+1)(2L+1)(2\Sigma'+1)(2\Sigma+1)30}{(2S+3)(2S+1)(S+1)(2S-1)S}} \\
&\qquad \times (f_0^{2(\mathrm{P_S})} D^2_{0,K'-K}[\alpha_{P_SM}, \beta_{P_SM}, 0] \\
&\qquad + f_{|2|}^{2(\mathrm{P_S})} (D^2_{2,K'-K}[\alpha_{P_SM}, \beta_{P_SM}, 0] \\
&\qquad + D^2_{-2,K'-K}[\alpha_{P_SM}, \beta_{P_SM}, 0])) \\
&\qquad \times \begin{pmatrix} L' & 2 & L \\ -K' & K'-K & K \end{pmatrix} \begin{pmatrix} L' & 2 & L \\ -M' & M'-M & M \end{pmatrix} \\
&\qquad \times \begin{pmatrix} \Sigma' & 2 & \Sigma \\ -\sigma' & M-M' & \sigma \end{pmatrix} \begin{Bmatrix} \Sigma' & 2 & \Sigma \\ S & S & S \end{Bmatrix}, \qquad [A.1]
\end{aligned}
$$

$$
\begin{aligned}
&(A'B'C'|(L'K'M'|(\Sigma'\sigma'|\mathcal{L}^{\mathrm{T}}_{\mathrm{ZFS}}|\Sigma\sigma)|LKM)|ABC) \\
&\quad = (-1)^{\sigma+B'+K'-C'-M'} h^{2(P_T)}_{|B'-B|} \times \sqrt{5}((-1)^{\Sigma'+2+\Sigma}-1) \\
&\qquad \times \sqrt{\frac{(2A'+1)(2A+1)(2L'+1)(2L+1)}{\times (2\Sigma'+1)(2\Sigma+1)30}{(2S+3)(2S+1)(S+1)(2S-1)S}} \\
&\qquad \times \begin{pmatrix} A' & 2 & A \\ -B' & B'-B & B \end{pmatrix} \begin{pmatrix} A' & 2 & A \\ -C' & C'-C & C \end{pmatrix} \\
&\qquad \times \begin{pmatrix} L' & 2 & L \\ -K' & C'-C & K \end{pmatrix} \begin{pmatrix} L' & 2 & L \\ -M' & M'-M & M \end{pmatrix} \\
&\qquad \times \begin{pmatrix} \Sigma' & 2 & \Sigma \\ -\sigma' & M-M' & \sigma \end{pmatrix} \begin{Bmatrix} \Sigma' & 2 & \Sigma \\ S & S & S \end{Bmatrix}, \qquad [A.2]
\end{aligned}
$$

where

$$
\begin{Bmatrix} \Sigma' & 2 & \Sigma \\ S & S & S \end{Bmatrix}
$$

in Eqs. [A.1] and [A.2] is a 6-j symbol (*59*). If the Liouville superoperator contains electron spin operators of rank two, as in Eqs. [A.1] and [A.2], then there is a general selection rule

$$
|\Sigma' - \Sigma| = 1. \qquad [A.3]
$$

This selection rule originates from the inversion conjugation symmetry (*60, 61*) and reduces the number of matrix elements that are non-zero.

ACKNOWLEDGMENTS

This work has been supported by the Swedish Natural Science Research Council. Generous grants of computer time by the Center for Parallel Computers in Stockholm are gratefully acknowledged.

REFERENCES

1. R. A. Dwek, "Nuclear Magnetic Resonance in Biochemistry," Clarendon, Oxford (1975).
2. D. R. Burton, S. Forsén, G. Karlström, and R. A. Dwek, Proton relaxation enhancement (PRE) in biochemistry: A critical survey, *Prog. NMR Spectrosc.* **13,** 1–45 (1979).
3. J. Kowalewski, L. Nordenskiöld, N. Benetis, and P.-O. Westlund, Theory of nuclear spin relaxation in paramagnetic systems in solution, *Prog. NMR Spectrosc.* **17,** 141–185 (1985).
4. L. Banci, I. Bertini, and C. Luchinat, "Nuclear and Electron Relaxation," VCH, Weinheim (1991).
5. P.-O. Westlund, Nuclear paramagnetic spin relaxation theory: Paramagnetic spin probes in homogeneous and microheterogeneous solutions, *in* "Dynamics of Solutions and Fluid Mixtures by NMR" (J. J. Delpuech, Ed.), Chap. 4, pp. 173–229, Wiley, Chichester (1995).
6. I. Solomon, Relaxation processes in a system of two spins, *Phys. Rev.* **99,** 559–565 (1955).
7. I. Solomon and N. Bloembergen, Nuclear magnetic interactions in the HF molecule, *J. Chem. Phys.* **25,** 261–266 (1956).
8. N. Bloembergen, Proton relaxation times in paramagnetic solutions, *J. Chem. Phys.* **27,** 572–573 (1957).
9. N. Bloembergen and L. O. Morgan, Proton relaxation times in paramagnetic solutions: Effects of electron spin relaxation, *J. Chem. Phys.* **34,** 842–850 (1961).
10. E. Strandberg and P.-O. Westlund, Paramagnetic proton nuclear spin relaxation theory of low-symmetry complexes for electron spin quantum number $S = 5/2$, *J. Magn. Reson.* **137,** 333–344 (1999).
11. N. Benetis, J. Kowalewski, L. Nordenskiöld, H. Wennerström, and P.-O. Westlund, Nuclear spin relaxation in paramagnetic systems: The slow motion problem for the electron spin relaxation, *Mol. Phys.* **48,** 329–346 (1983).
12. N. Benetis, J. Kowalewski, L. Nordenskiöld, H. Wennerström, and P.-O. Westlund, Dipole–dipole nuclear spin relaxation: A cross correlation correction to the Solomon–Bloembergen equation for T_2, *Mol. Phys.* **50,** 515–530 (1983).
13. N. Benetis, J. Kowalewski, L. Nordenskiöld, H. Wennerström, and P.-O. Westlund, Nuclear spin relaxation in paramagnetic systems ($S = 1$) in the slow-motion regime for the electron spin: II. The dipolar T_2 and the role of scalar interaction, *J. Magn. Reson.* **58,** 261–281 (1984).
14. P.-O. Westlund, H. Wennerström, L. Nordenskiöld, J. Kowalewski, and N. Benetis, Nuclear spin–lattice and spin–spin relaxation in paramagnetic systems in the slow-motion regime for the electron spin: III. Dipole–dipole and scalar spin–spin interaction for $S = 3/2$ and $S = 5/2$, *J. Magn. Reson.* **59,** 91–109 (1984).
15. N. Benetis and J. Kowalewski, Nuclear spin relaxation in paramagnetic systems ($S = 1$) in the slow-motion regime for the electron spin: IV. Motional anisotropy and noncoinciding dipole–dipole and zero-field splitting tensors, *J. Magn. Reson.* **65,** 13–33 (1985).
16. L. T. Muus and P. W. Atkins, Eds., "Electron Spin Relaxation in Liquids," Plenum, New York (1972).
17. J. Jeener, Superoperators in magnetic resonance, *Adv. Magn. Reson.* **10,** 1–51 (1982).
18. R. K. Wangsness and F. Bloch, The dynamical theory of nuclear induction, *Phys. Rev.* **89,** 728–739 (1953).

19. F. Bloch, Dynamical theory of nuclear induction. II, *Phys. Rev.* **102,** 104–135 (1956).
20. A. G. Redfield, On the theory of relaxation processes, *IBM J. Res. Dev.* **1,** 19–31 (1957).
21. A. G. Redfield, The theory of relaxation processes, *Adv. Magn. Reson.* **1,** 1–32 (1965).
22. C. P. Slichter, "Principles of Magnetic Resonance," 3rd ed., Springer Verlag, Berlin (1992).
23. T. Nilsson, J. Svoboda, P.-O. Westlund, and J. Kowalewski, Slow-motion theory of nuclear spin relaxation in paramagnetic complexes ($S = 1$) of arbitrary symmetry, *J. Chem. Phys.* **109,** 6364–6375 (1998).
24. H. Fukui, K. Miura, and H. Matsuda, The rhombic effect of zero-field splitting on the nuclear relaxation times: Quenching of the electron spin angular momentum, *J. Magn. Reson.* **88,** 311–319 (1990).
25. R. R. Sharp, Nuclear spin relaxation due to paramagnetic species in solution: Effect of anisotropy in the zero field splitting tensor, *J. Chem. Phys.* **98,** 6092–6101 (1993).
26. J.-M. Bovet and R. R. Sharp, Nuclear magnetic resonance relaxation enhancements produced by paramagnetic solutes: Effects of rhombicity in the zero field splitting tensor with the $S = 2$ spin system as an example, *J. Chem. Phys.* **99,** 18–26 (1993).
27. S. M. Abernathy, J. C. Miller, L. L. Lohr, and R. R. Sharp, Nuclear magnetic resonance–paramagnetic relaxation enhancements: Influence of spatial quantization of the electron spin when the zero-field splitting energy is larger than the Zeeman energy, *J. Chem. Phys.* **109,** 4035–4046 (1998).
28. U. Lindner, Protonenrelaxation in paramagnetischen lösungen unter berücksichtigung der nullfeldaufspaltung, *Ann. Phys. (Leipzig)* **16,** 319–335 (1965).
29. I. Bertini, C. Luchinat, M. Mancini, and G. Spina, The electron–nucleus dipolar coupling: The effect of zero-field splitting of an $S = 3/2$ manifold, *J. Magn. Reson.* **59,** 213–222 (1984).
30. R. R. Sharp, Effect of zero field splitting interactions on the paramagnetic relaxation enhancement of nuclear spin relaxation rates in solution, *J. Chem. Phys.* **98,** 912–921 (1993).
31. R. R. Sharp, Characteristic properties of the nuclear magnetic resonance–paramagnetic relaxation enhancement arising from integer and half-integer electron spins, *J. Chem. Phys.* **98,** 2507–2515 (1993).
32. L. Banci, I. Bertini, F. Briganti, and C. Luchinat, The electron–nucleus dipolar coupling in slow rotating systems: 4. The effect of zero-field splitting and hyperfine coupling when $S = 5/2$ and $I = 5/2$, *J. Magn. Reson.* **66,** 58–65 (1986).
33. I. Bertini, O. Galas, C. Luchinat, and G. Parigi, A computer program for the calculation of paramagnetic enhancements of nuclear-relaxation rates in slowly rotating systems, *J. Magn. Reson. Ser. A* **113,** 151–158 (1995).
34. R. Kubo and K. Tomita, A general theory of magnetic resonance absorption, *J. Phys. Soc. Jpn.* **9,** 888–919 (1954).
35. I. Bertini, J. Kowalewski, C. Luchinat, T. Nilsson, and G. Parigi, Nuclear spin relaxation in paramagnetic complexes of $S = 1$: Electron spin relaxation effects, *J. Chem. Phys.* **111,** 5795–5807 (1999).
36. P. O. Westlund, A low-field paramagnetic nuclear spin relaxation theory, *J. Chem. Phys.* **108,** 4945–4953 (1998).
37. T. Bayburt and R. R. Sharp, Electron- and nuclear-spin relaxation in an integer spin system, tris-(ascetylacetonato)Mn(III) in solution, *J. Chem. Phys.* **92,** 5892–5899 (1990).
38. R. R. Sharp, Nuclear spin relaxation in paramagnetic solutions: Effects of large zero-field splitting in the electron spin Hamiltonian, *J. Chem. Phys.* **93,** 6921–6928 (1990).
39. R. R. Sharp, Nuclear-spin relaxation in paramagnetic solutions when the electronic zero-field splitting and Zeeman interactions are of arbitrary magnitude, *J. Magn. Reson.* **100,** 491–516 (1992).
40. R. Sharp, S. M. Abernathy, and L. L. Lohr, Paramagnetically induced nuclear magnetic resonance relaxation in solutions containing $S \geq 1$ ions: A molecular-frame theoretical and physical model, *J. Chem. Phys.* **107,** 7620–7629 (1997).
41. S. M. Abernathy and R. R. Sharp, Spin dynamics calculations of electron and nuclear spin relaxation times in paramagnetic solutions, *J. Chem. Phys.* **106,** 9032–9043 (1997).
42. J. Svoboda, T. Nilsson, J. Kowalewski, P.-O. Westlund, and P. T. Larsson, Field-dependent proton NMR relaxation in aqueous solutions of Ni(II) ions: A new interpretation, *J. Magn. Reson. Ser. A* **121,** 108–113 (1996).
43. P.-O. Westlund, N. Benetis, and H. Wennerström, Paramagnetic proton nuclear magnetic relaxation in the Ni^{2+} hexa-aquo complex: A theoretical study, *Mol. Phys.* **61,** 177–194 (1987).
44. P.-O. Westlund and P. T. Larsson, Proton-enhanced relaxation in low-symmetry paramagnetic complexes ($S = 1$): Beyond the Solomon–Bloembergen and Morgan theory. 1. The Smoluchowski distortion model of the ZFS interaction, *Acta Chem. Scand.* **45,** 11–18 (1991).
45. P.-O. Westlund, T. P. Larsson, and O. Teleman, Paramagnetic enhanced proton spin–lattice relaxation in the Ni^{2+} hexa–aquo complex: A theoretical and molecular dynamics simulation study of the Bloembergen–Morgan decomposition approach, *Mol. Phys.* **78,** 1365–1384 (1993).
46. T. Larsson, P.-O. Westlund, J. Kowalewski, and S. H. Koenig, Nuclear-spin relaxation in paramagnetic complexes in the slow-motion regime for the electron spin: The anisotropic pseudorotation model for $S = 1$ and the interpretation of nuclear magnetic relaxation dispersion results for a low-symmetry Ni(II) complex, *J. Chem. Phys.* **101,** 1116–1128 (1994).
47. D. M. Brink and G. R. Satchler, "Angular Momentum," 2nd ed., Clarendon, Oxford (1979).
48. K. Blum, "Density Matrix Theory and Applications," Plenum, New York (1989).
49. R. Kubo, Stochastic Liouville equations, *J. Math. Phys.* **4,** 174–183 (1963).
50. J. H. Freed, G. V. Bruno, and C. Polnaszek, ESR line shapes for triplets undergoing slow rotational reorientation, *J. Chem. Phys.* **55,** 5270–5281 (1971).
51. J. H. Freed, G. V. Bruno, and C. F. Polnaszek, Electron spin resonance line shapes and saturation in the slow motional region, *J. Phys. Chem.* **75,** 3385–3399 (1971).
52. M. Odelius, C. Ribbing, and J. Kowalewski, Molecular dynamics simulation of the zero-field splitting fluctuations in aqueous Ni(II), *J. Chem. Phys.* **103,** 1800–1811 (1995).
53. M. Odelius, C. Ribbing, and J. Kowalewski, Spin dynamics under the Hamiltonian varying with time in descrete steps: Molecular dynamics-based simulation of electron and nuclear spin relaxation in aqueous nickel(II), *J. Chem. Phys.* **104,** 3181–3188 (1996).
54. A. Abragam and B. Bleaney, "Electron Paramagnetic Resonance of Transition Ions," Clarendon, Oxford (1970).

55. W. Low, Paramagnetic resonances in solids, *in* "Solid State Physics, Supplement 2" (F. Seitz and D. Turnbull, Eds.), Academic Press, New York (1960).

56. J. E. Wertz and J. R. Bolton, "Electron Spin Resonance: Elementary Theory and Practical Applications," McGraw–Hill, New York (1972).

57. C. Lanczos, Solution of systems of linear equations by minimized iterations, *J. Res. Natl. Bur. Stand.* **49,** 33–53 (1952).

58. T. Nilsson and J. Kowalewski, Low-field theory of nuclear spin relaxation in paramagnetic low-symmetry complexes with electron spin systems of $S = 1, 3/2, 2, 5/2, 3$, and 7/2, *Mol. Phys.,* in press (2000).

59. M. Rotenberg, R. Bivins, N. Metropolis, and J. K. Wooten, "The 3-J and 6-J Symbols," Technology Press, Cambridge (1959).

60. N. C. Pyper, Theory of symmetry in nuclear magnetic relaxation including applications to high resolution NMR line shapes, *Mol. Phys.* **21,** 1–33 (1971).

61. R. M. Lynden-Bell, A density matrix formulation of the theory of magnetic resonance spectra in slowly reorienting systems, *Mol. Phys.* **22,** 837–851 (1971).